Multi-physics modeling of an active seat suspension with pneumatic or hydraulic actuation

M.G. Antonelli [1], **J. Brunetti** [1], **W. D'Ambrogio** [1], **A. Fregolent** [2], **F. Latini** [2]
[1] Università dell'Aquila, Dipartimento di Ingegneria Industriale e dell'Informazione e di Economia,
Via G. Gronchi 18, 67100 L'Aquila (AQ), Italy
e-mail: **jacopo.brunetti@univaq.it**

[2] Università di Roma La Sapienza, Dipartimento di Ingegneria Meccanica e Aerospaziale,
Via Eudossiana 18, 00184 Rome, Italy

Abstract
Vertical vibrations on agricultural tractors, due to soil irregularities, represent a major cause of diseases of agricultural operators. The control of noise and vibration on the operator is of interest to the (Italian) National Institute for Insurance against Accidents at Work (INAIL). Several systems for the seat or cabin suspension are commercially available to reduce the transmitted vibrations. The state of the art of suspension systems includes passive, semi-active and active solutions. A prototype of an active suspension system of the operator seat has been developed in the laboratories of INAIL. The prototype has the peculiarity that it can be configured with hydraulic or pneumatic actuation. In order to develop and optimize the control system, multi-physics modeling of both configurations has been carried out and described in this paper. The hydraulic and pneumatic circuits as well as the two types of valves and the actuators are numerically modeled in the Simulink environment. The proposed models have been validated using experimental data.

1 Introduction

Vertical vibrations on agricultural tractors, due to soil irregularities, represent a major cause of diseases of agricultural operators. A broad literature exists on the effects of whole-body vibrations exposure on operators of industrial and agricultural machines [1, 2, 3, 4, 5, 6]. The control of noise and vibration on the operator is of interest to the (Italian) National Institute for Insurance against Accidents at Work (INAIL). Several systems for the seat or cabin suspension are commercially available to reduce the transmitted vibrations including either passive, semi-active or active solutions. Passive solutions are typically mechanical [7] or pneumatic [8] and generally allow for an attenuation of the vibrations beyond a given cut-off frequency. Semi-active solutions typically adjust the damping coefficient to adapt the response of the system to the excitation due to soil irregularities [9, 10]. They guarantee better performances with respect to the passive isolation systems, but they typically require the use of sensors and an electronic control unit. Active solutions are characterized by the presence of an actuation system based on hydraulic, direct-drive electromagnetic, electromagnetic hydrostatic or geared electric motor technology [11, 12, 13].

A prototype of an active suspension system of the operator seat has been developed in the laboratories of INAIL. The prototype has the peculiarity that it can be configured with hydraulic or pneumatic actuation. In the former configuration, the system includes a hydraulic cylinder powered by a proportional flow-rate control electro-valve. In the latter, the pneumatic cylinder is powered by a proportional pressure control electro-valve. Both technologies are evaluated because of the presence of either the hydraulic and pneumatic power supply on board of an agricultural machine. The hydraulic solution provides a very high power to weight ratio and a precise position control. However, this solution makes the suspension rigid, the mineral oil is pollutant and components and maintenance might be quite expensive. On the other hand, the pneumatic solution (cheap, clean, with high power to weight ratio) exploits the air available in the environment and

behaves as an air spring attenuating low frequency excitation. In the pneumatic case, the pressure control valves allow for force control and a variable stiffness actuation (VSA) [14, 15]. Nevertheless, this system requires suitable strategies for precise position control due to the compressibility of the air.

Multi-physics modeling of both hydraulic and pneumatic configurations is carried out and described in this paper. The hydraulic and pneumatic circuits as well as the two types of valves and the actuators are numerically modeled in the Simulink environment. Each model aims at providing a reliable simulator for the development and optimization of the control system. Experimental test are performed on the hydraulic active suspension and the responses of the system are compared with those provided by the numerical model. Regarding the pneumatic suspension, a reduced scale system is built. Preliminary tests are performed to characterize the model of the electro-valve that is introduced in the numerical model of the suspension system. Subsequent tests are performed on the complete pneumatic system, and also in this case the responses are compared with those provided by the numerical model.

2 Prototype of an agricultural machine seat suspension

The prototype of the agricultural machine seat suspension is made of the only actuation system placed on the vibrating frame as shown in Figure 1.

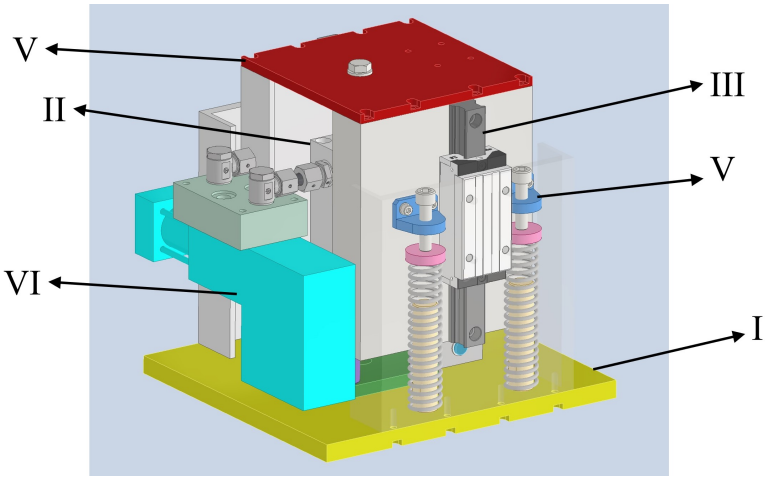

Figure 1: Prototype of the seat suspension.

As shown in Figure, the actuation system is mounted over the vibrating platform (I) and it is composed of the actuator (II), the sliders (III), the suspended body (IV), a set of springs (V) the electro-valve (VI), a linear position transducer and a couple of accelerometers. The actuator can be either hydraulic (ISO 6020 double through rod, bore 25 mm, stroke 70 mm) or pneumatic (ISO 21287 double acting, bore 80 mm, stroke 70 mm) and it is mounted along the vertical axis. The upper end of the rod is bolted to the suspended body and provides for its motion. The sliders are recirculating ball bearing guides that guarantee the vertical motion avoiding any transversal loads on the rod. The electro-valve is a proportional flow-rate control valve in the hydraulic case (Duplomatic DXJ3-DOL20/10N/E0K11, maximum flow rate of 20 l/min), or a proportional pressure control valve in the pneumatic one (Festo VPPN-6F-L-1-F-0L6H-A4N-S1 maximum flow rate 1000 l/min). The system is connected to a supply line with a feed pressure equal to 100 bar in the hydraulic case and 6 bar in the pneumatic one. The suspended body is composed of aluminum parts and the upper plate is designed to support the operator's seat or an equivalent mock-up. A set of four springs (D13420MW, stiffness 3680 N/m each, free length 200 mm) is placed to support the static load of the suspended body plus the seat and operator. The linear position transducer is a resistive type (Gefran PZ34-A-075, stroke 75 mm) and measures the displacement of the suspended body with respect to the vibrating frame. The accelerometers are MEMS type (GY-61 DXL335, full scale range $\pm$3g, bandwidth 0.5-550 Hz, in the vertical direction): one is placed over the vibrating frame an the other is placed over the upper plate.

3 Active suspension system modeling

Depending on the type of actuation system, two models of the active suspension systems are developed: the hydraulic one is referred to a cylinder powered by the proportional flow-rate control valve while the pneumatic one is referred to a cylinder powered by a proportional pressure control valves. In the next Sections, both models are detailed and described.

3.1 Hydraulic actuation

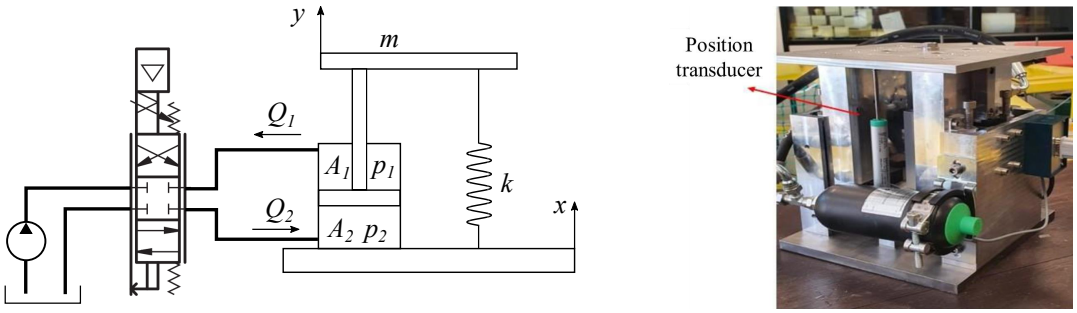

Figure 2: Schematic and testbed of the hydraulic active suspension.

Figure 2 show the schematic and the tesbed of the hydraulic active suspension. The set of thirteen equations is reported: the dynamic equilibrium equation of the seat Eq. (1), the equations for pipelines 1 and 2 Eqs. (2–7), the equations of the hydraulic resistance, inertance and capacitance Eqs. (8–10), the equation for the inlet and outlet flow rates through the valve Eqs. (11–12), the equilibrium equation of the spool of the valve Eq. (13).

$$m\ddot{y} + k(y - x) + p_1 A_1 - p_2 A_2 = 0 \tag{1}$$

where y is the displacement of the seat, x is the disturbance at the base of the system, m is the suspended mass, k is the equivalent stiffness of set of springs, p_i is the pressure and A_i is the cross section of the cylinder chamber.

$$p_1 - p_{1v} = R_1 Q_1 + I_1 \dot{Q}_1 \tag{2}$$
$$p_{2v} - p_2 = R_2 Q_2 + I_2 \dot{Q}_2 \tag{3}$$
$$Q_1 = \dot{u} A_1 - C_1 \dot{p}_1 \tag{4}$$
$$Q_2 = \dot{u} A_2 - C_2 \dot{p}_2 \tag{5}$$
$$Q_1 - Q_{1v} = C_{1c} \dot{p}_{1v} \tag{6}$$
$$Q_{2v} - Q_2 = C_{2c} \dot{p}_{2v} \tag{7}$$

where Q_i is the volumetric flow-rate and $u = y - x$ is the relative displacement. The hydraulic resistance R_i, inertance I_i and capacitance C_i are defined as:

$$R_i = \frac{128 \mu L_i}{\pi d_i^4} \tag{8}$$
$$I_i = \frac{4 \rho L_i}{\pi d_i^2} \tag{9}$$
$$C_i = \frac{\pi L_i d_i^2}{4 \beta} \tag{10}$$

where ρ, μ and β are the density, the compressibility modulus and the dynamic viscosity of the mineral oil, respectively; L and d are the length and diameter of the pipeline, respectively.

$$Q_{1v} = \begin{cases} C_d k_a x_v \sqrt{\frac{2}{\rho}(p_{1v} - p_0)} & \text{if} \quad x_v > 0 \\ C_d k_a x_v \sqrt{\frac{2}{\rho}(p_A - p_{1v})} & \text{if} \quad x_v \leq 0 \end{cases} \tag{11}$$

$$Q_{2v} = \begin{cases} C_d k_a x_v \sqrt{\frac{2}{\rho}(p_A - p_{2v})} & \text{if} \quad x_v > 0 \\ C_d k_a x_v \sqrt{\frac{2}{\rho}(p_{2v} - p_0)} & \text{if} \quad x_v \leq 0 \end{cases} \tag{12}$$

where C_d is the flow coefficient, x_v is the displacement of the spool and $k_a x_v$ is the cross section of the hydraulic valve.

$$\ddot{x_v} + 2\zeta\omega_n \dot{x_v} + \omega_n^2 x_v = \omega_n^2 k_v V_{in} \tag{13}$$

where k_v is the static gain of the proportional valve, ω_n, ζ are the natural frequency and damping ratio of the proportional valve and V_{in} is the command tension, which is bounded to $\pm$10 V.

The values of the parameters used in the Eqs. (1–13) are listed in Table 1. Note that, the flow coefficient C_d is estimated, as suggested by the valve manufacturer, using Eq. (11) with the nominal operating conditions of the valve, i.e. Q=20 l/min and Δp=70 bar and considering the completely open position of the valve. Thus, the hydraulic dynamic system can be described by ten state-variables and two input variables (V_{in} and x).

Table 1: Parameters of the hydraulic model. All data are expressed in SI units.

m	k	p_A	p_0	β	ρ	μ	A_i	d_i	L_i	k_a	k_v	C_d
11.7	3680	100e06	1e06	1.2e09	840	0.02	2.36e-04	0.01	0.5	2.51e-02	8e-05	0.1074

3.2 Pneumatic actuation

The pneumatic active suspension, shown in Figure 3, is made of a proportional pressure control valve connected to the lowest chamber (the posterior one) of the cylinder, a pressure regulator connected to the highest chamber (the anterior one), an additional plenum connected to the anterior chamber, a wire linear position transducer (Celesco DV301-0020-111-1110) connected to the end of the rod and two pressure transducers (Gefran TKDA-N-I-E-B01D-H-Y) connected to the two chambers. The adoption of the additional plenum prevents from exceeding a pressure of 0.6 MPa in the anterior chamber. A one-way valve is connected to the anterior chamber to avoid the air outlet from it. At the end of the rod, a mass of 5 kg is placed.

The pneumatic system is experimentally tested, and a simplified numerical model of it is implemented. A set of three equations is adopted to model the pneumatic system: the dynamic equilibrium equation of the moving masses of the cylinder (14); the equation of the pressure P_1 (expressed in MPa) in the posterior chamber (15); the equation of the pressure P_2 (expressed in MPa) in the anterior chamber (16).

$$P_1 A_1 - P_2 A_2 - M\ddot{x} - Mg - c_f \dot{x} + F_0 - Kx = 0 \tag{14}$$

where A_1 and A_2 are the cross-sections (expressed in mm^2) of the piston in the posterior and anterior chambers, respectively; M is the overall mass of the moving parts, including the external mass applied to the end of the rod; c_f is the damping constant (expressed in Ns/m) of the friction force, modeled as a viscous force; F_0 is the elastic force (expressed in N) applied by the wire position transducer to the rod when the stroke of

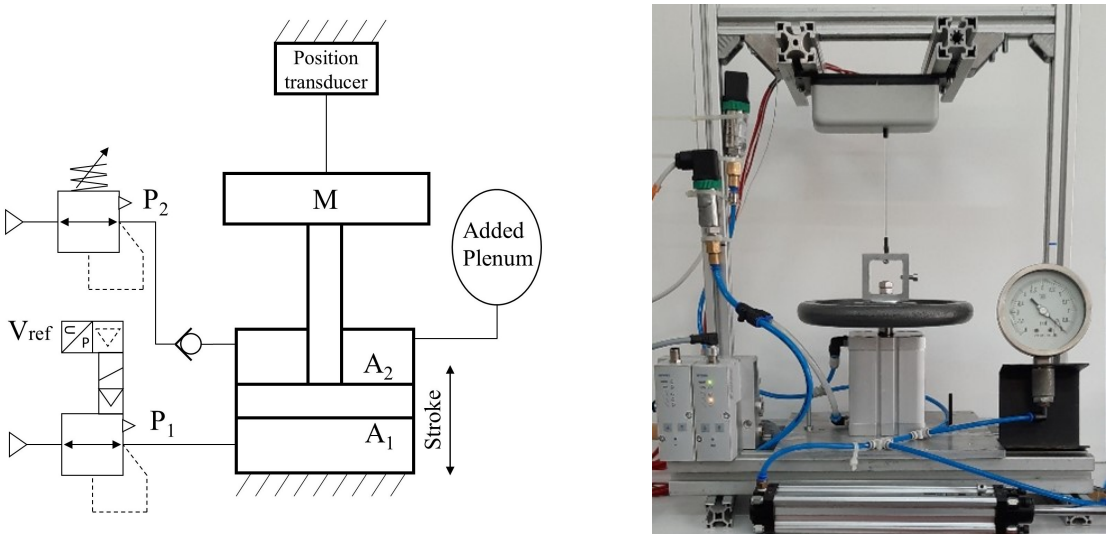

(a) Schematic of the pneumatic system.

(b) Experimental pneumatic test bed.

Figure 3: Schematic and testbed of the pneumatic active suspension.

the rod x is null; K (expressed in N/m) is the equivalent linear elastic constant of the torsional spring of the rolling drum where the wire is wrapped.

The dynamic behavior of a proportional pressure control valve can be described, with a good approximation, by the following second-order equation [16]:

$$\ddot{P}_1 + 2\zeta\omega_n\dot{P}_1 + \omega_n^2 P_1 = \omega_n^2 K_S\left(V_{ref} - V_0\right) \tag{15}$$

where P_1 is the relative pressure (measured in MPa) in the posterior chamber provided by the valve; ζ and ω_n are the damping ratio and the natural frequency, respectively; K_S is the static gain (equal to 0.143 MPa/V); V_{ref} and V_0 are the command tension and the offset tension (1 Vdc), respectively.

$$P_2 = P_{20}\left(1 - \frac{A_2 x}{V_0}\right)^{-\gamma} \tag{16}$$

where P_{20} is the pressure value (expressed in MPa) in the anterior chamber at the initial condition; V_0 is the whole volume of air of the anterior chamber, the additional plenum and the pneumatic piping; γ is the isentropic index (equal to 1.4). The values of the parameters of Eqs. (14)–(16) are reported in Table 2.

Table 2: Parameters of the pneumatic model.

A_1 [mm^2]	A_2 [mm^2]	M [kg]	c_f [Ns/m]	F_0 [N]	K [N/m]	V_0 [mm^3]	K_s [MPa/V]	V_{off} [Vdc]
5.02e+03	4.71e+3	5.6	200	7	70	5.03e+05	0.143	1

4 Experimental validation of the actuation systems' models

The models described in the previous section are developed in order to have a virtual system for the active control development. Therefore, several tests are performed on both the hydraulic and pneumatic systems in order to validate the dynamic models. In particular, for the pneumatic system an experimental characterization and validation of the valve model is performed.

4.1 Hydraulic system

The hydraulic system is tested by imposing a given signal to the command tension $V_{in}(t)$ of the electrovalve, the vibrating frame is kept still during tests ($x(t) = 0$). The response of the system is measured using the MEMS accelerometer placed on the suspended plate $\ddot{y}$, and the resistive linear position transducer between the base frame and suspended plate $u(t)$.

Figure 4 shows the three different square-wave signals imposed on the electrovalve. In particular, the three signals have an amplitude of 0.82, 0.54 and 0.26 V and a frequency of 1.25, 0.63 and 0.42 Hz, respectively.

Since a proportional flow-rate control valve is used in the hydraulic case, the displacement response to a square wave on the control tension of the valve is expected to be a sawtooth wave. The same signals are used also to evaluate the response of the numerical model. Figure 5 shows a comparison of the measured response of the hydraulic system (continuous lines) with the response provided by the model (dashed lines) for the three command signals. The displacement response provided by the model, using the parameters in

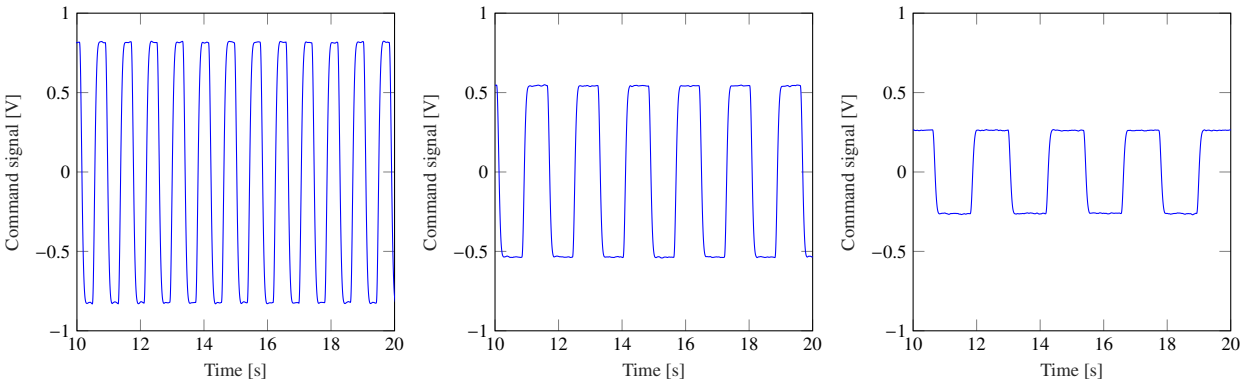

(a) Case 1 (b) Case 2 (c) Case 3

Figure 4: Command signals imposed on the the electrovalve of hydraulic system.

Table 1, is almost the same for the Case 3, that is the case with the lowest amplitude and frequency. However,

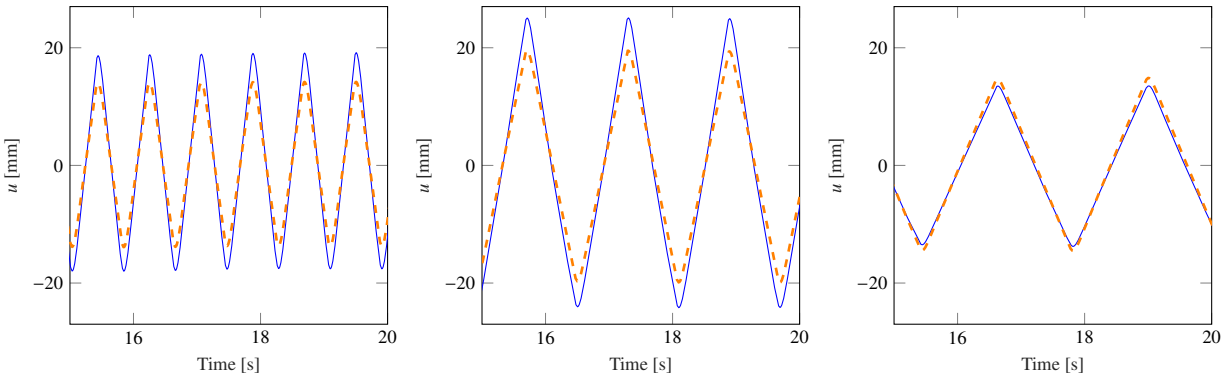

(a) Case 1 (b) Case 2 (c) Case 3

Figure 5: Numerical and experimental response of the hydraulic system. Experimental (——); Numerical (- - -)

the model underestimates the amplitude of the response for the other two cases. To understand the reason of this discrepancy the numerical and experimental displacement signals are numerically derived to obtain the velocity. Figure 6 shows a comparison of the vertical velocity of the suspended mass of the hydraulic system (continuous lines) with the velocity provided by the model (dashed lines) for the three command signals. Results highlight that at the lowest frequency the numerical model provides a slightly higher value

of the velocity. However, by increasing the frequency of the command signal the model underestimates the velocity and therefore the displacement of the suspended mass. Moreover, the experimental responses show that for a constant value of the command signal the velocity is not constant as it would be expected by using a proportional flow-rate electrovalve. This aspect is particularly evident for Case 2 where the the velocity exhibits a positive slope in correspondence of a constant value of the command signal. It is not clear at this point the reason of this underestimation and a campaign of systematic tests should be performed to understand if it is a frequency or amplitude related phenomenon that should be accounted for in the numerical model.

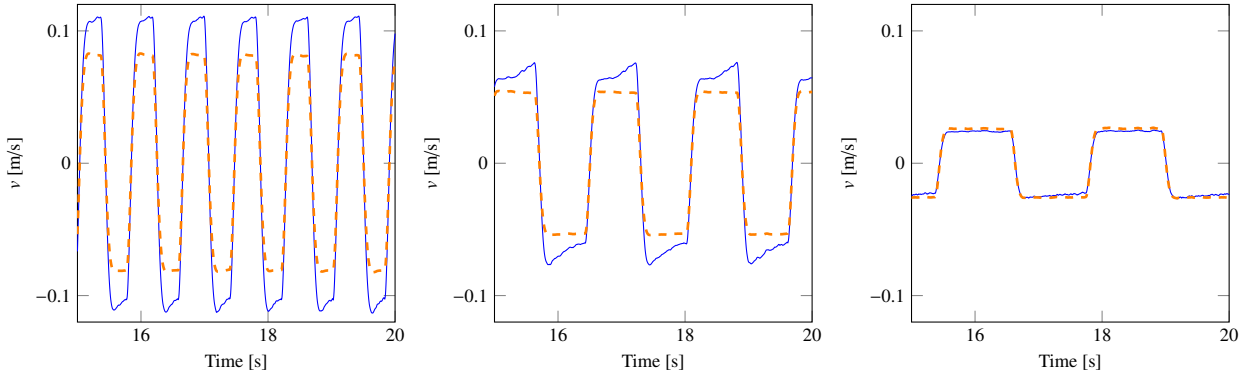

(a) Case 1 (b) Case 2 (c) Case 3

Figure 6: Numerical and experimental velocity of the hydraulic system. Experimental (——); Numerical (- - -)

4.2 Pneumatic system

A preliminary dynamic experimental test are conducted to characterize the adopted proportional pressure control valve. The output pressure ranges from 0–0.6 MPa. Although the output pressure is proportional to an input command current, which ranges from 4–20 mA, the valve is commanded by an equivalent command tension, which ranges from 1–5 Vdc. The valve can work according to three functional modes: fast, universal, and precise control behavior. In the presented activity, the valve is set to the universal control behavior mode.

To achieve the dynamic parameters ζ and ω_n, a command signal V_{ref} made of a sine wave with amplitude 1.10 V and offset 3.60 Vdc (corresponding to an amplitude of 0.16 MPa and an offset pressure of 0.38 MPa) is imposed to the valve. Maintaining constant amplitude and offset, tests are carried out at different frequencies in the range of 0.2–20 Hz. A signal generator (GW Instek AFG-2125) is used for the command tension. A data acquisition system, made of a USB NI6001 DAQ-board (14-bit resolution) and a personal computer running a software developed in the NI LabView environment, is adopted to acquire the command signal V_{ref}, converted into the corresponding pressure set-point, and the output pressure value P_{out} from the valve. The sampling frequency is set to 1 kHz.

As reported in Figure 7, from frequency values equal to 4 Hz, the shape of the output pressure signal differs from the sinusoidal shape of the input set-point: the amplitude is affected by attenuation more evident at higher frequencies. Moreover, a phase shift between the two curves occurs also at low-frequency values, starting from 0.5 Hz.

The magnitude and the phase shift of the output pressure with respect to the set-point, are achieved using the following criterion: at a given frequency, according to the nonlinear least-squares method, each of the two curves is described by an offset sine expressed by the equation:

$$y(t) = A + B\sin(2\pi ft + \varphi) \tag{17}$$

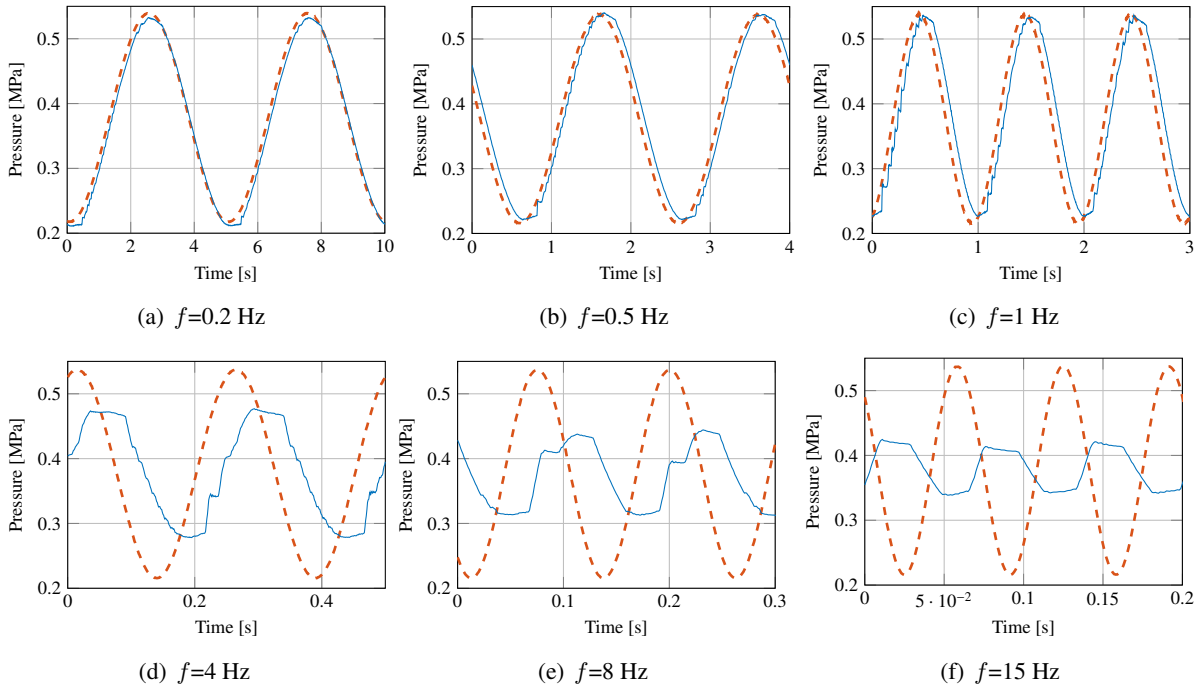

(a) f=0.2 Hz (b) f=0.5 Hz (c) f=1 Hz

(d) f=4 Hz (e) f=8 Hz (f) f=15 Hz

Figure 7: Comparison between set-point and output pressure values of the valve at different values of frequency f. Output pressure (——); Set-point (- - -).

where A is the identified offset value of the input/output (i/o) signal (in MPa), B is the identified amplitude of the signal (in MPa), f is the frequency of the input signal (in Hz), t is the time (in s), and φ is the identified phase of the signal. Hence, for each frequency value, the magnitude $|B_o/B_i|$ and the phase shift $\varphi_f = \varphi_o - \varphi_i$ are computed.

Some examples of identified input and output curves at various frequencies are reported in Figure 8.

The identified magnitude and phase shift are gathered in Figure 9.

The resonance frequency can be obtained by observing Figure 9(b), in fact when the phase shift is $-\pi/2$ the frequency value is $f_n = 7.16$ Hz, which corresponds to $\omega_n = 45$ rad/s. To identify the damping factor ζ the expression of the magnitude and the phase are considered:

$$|G(j\omega)| = \frac{1}{\sqrt{\left[1 - \left(\frac{\omega}{\omega_n}\right)^2\right]^2 + \left(2\zeta\frac{\omega}{\omega_n}\right)^2}} \tag{18}$$

$$\varphi = \arctan\left(\frac{2\zeta\frac{\omega}{\omega_n}}{1 - \left(\frac{\omega}{\omega_n}\right)^2}\right) \tag{19}$$

The best fit of the magnitude and the phase is achieved for a damping factor $\zeta = 1.2$ (Figure 9). The selected values for ζ and ω_n provide for a good approximation of the magnitude and the phase in the range 0–10 Hz ($\omega \simeq$ = 45 rad/s). Over this value, some visible differences occur also because the output pressure is not anymore harmonic. Therefore, the model of the dynamic behavior of the valve is:

$$\ddot{P}_{out} + 2 \cdot 1.2 \cdot 45\, \dot{P}_{out} + 45^2\, P_{out} = 45^2 \cdot 0.143\ (V_{ref} - 1) \quad \text{with} \quad V_{ref} = 1\text{–}5\,\text{Vdc} \tag{20}$$

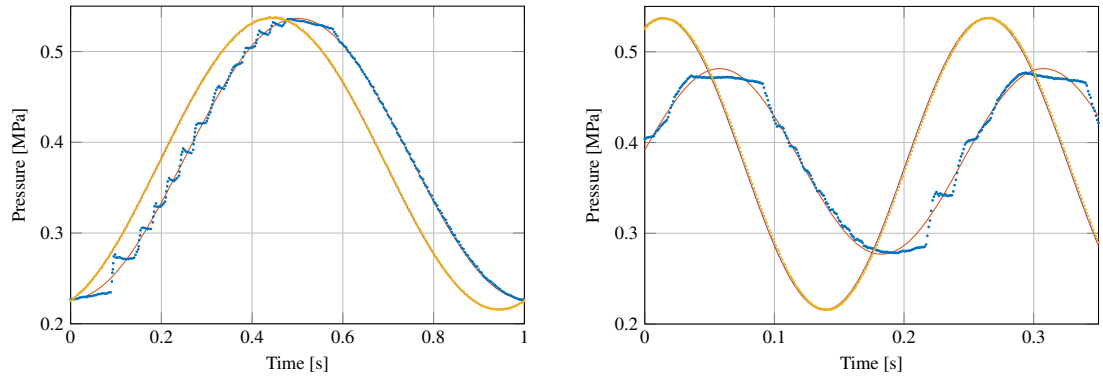

(a) f=1 Hz (b) f=4 Hz

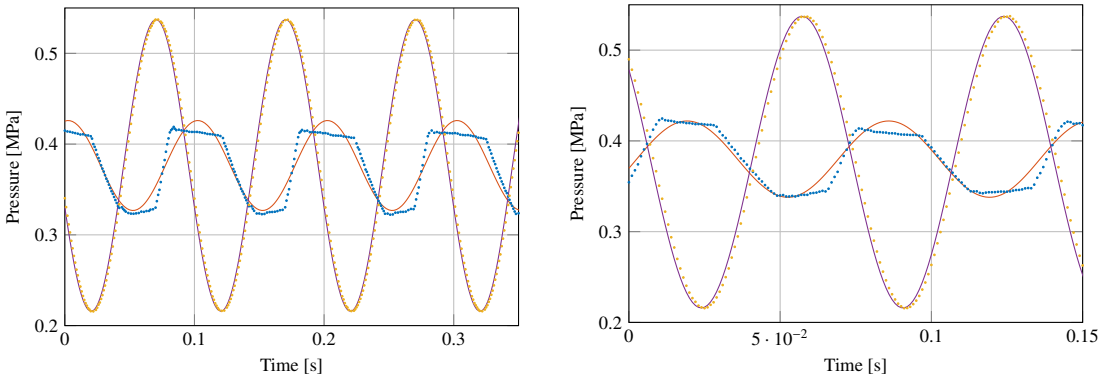

(c) f=8 Hz (d) f=15 Hz

Figure 8: Examples of identified input and output signals at different values of frequency f. Output (·····), Identified output (——), Input (·····), and Identified input (——).

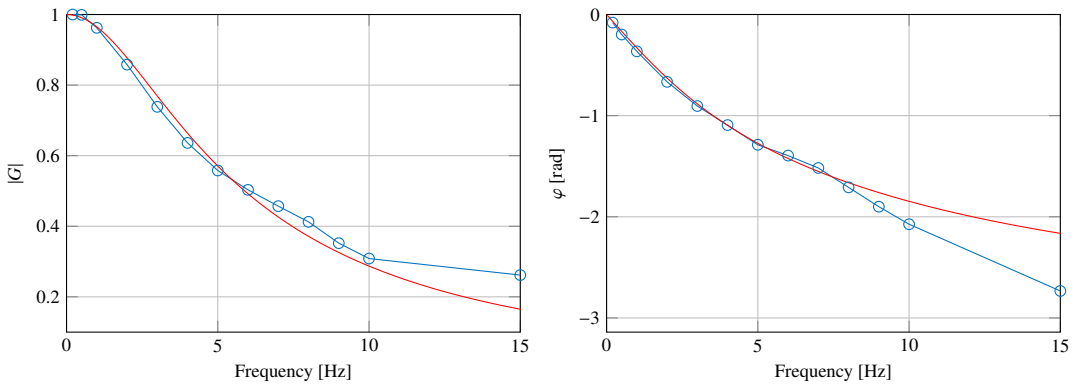

(a) Magnitude (b) Phase

Figure 9: Magnitude and phase of the proportional pressure valve response. Identified (–o–) and Fitted (——).

To validate the model of the valve, experimental data are compared to numerical results obtained by imposing the same experimental offset sine V_{ref} to the model. Figure 10 shows the compared curves, at different

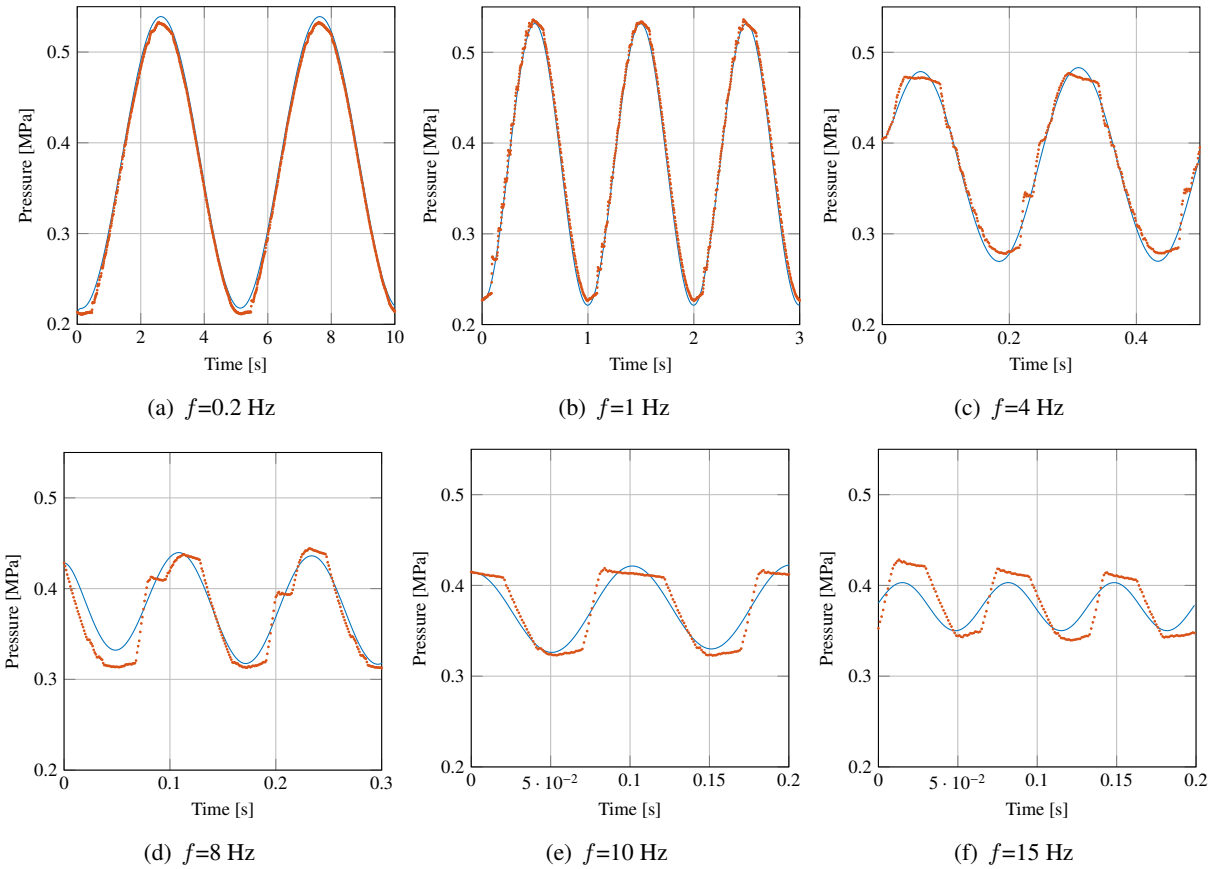

(a) f=0.2 Hz (b) f=1 Hz (c) f=4 Hz

(d) f=8 Hz (e) f=10 Hz (f) f=15 Hz

Figure 10: Comparison between experimental and numerical output pressure of the valve at different frequencies. Numerical (——) and Experimental (·····).

frequency values. The identified model fits the experimental curves until 8 Hz with a good approximation: numerical and experimental amplitudes are quite similar and no significant phase shift is noticed. At 15 Hz, amplitude differences and a phase shift between can be noticed. Such a result is coherent with the plots in Figure 9. The model of the valve provides reliable results in the range of 1–10 Hz.

However, the adopted valve, in the universal control behavior mode, is able to follow the set-point pressure for frequencies lower than 1 Hz (see Figure 9): negligible amplitude attenuation and low phase shift occur. For frequencies higher than 1 Hz, a progressive magnitude attenuation can be noticed: at 15 Hz, the output pressure amplitude is about 0.3 the set-point amplitude.

Once the model of the valve is identified, the pneumatic system is tested by imposing a given offset square wave signal V_{ref} to the electro-valve with an amplitude of 1.10 V and an offset of 3.60 Vdc (corresponding to an amplitude of 0.16 MPa and an offset pressure of 0.38 MPa) at different frequency values in the range 0.1–20 Hz. During the test, the pressure in the anterior chamber, at the initial condition when the stroke of the rod is null (lowest position of the piston), is fixed to 0.2 MPa. The signal generator and the DAQ are the same as for the the valve tests. In this case the acquired signals are: the input signal, the pressures in the two chambers of the actuator and the stroke of the rod.

Comparisons between the experimental and numerical strokes of the cylinder are reported in Figure 11. Results show that up to 1 Hz, no significant phase shift is noticed between the numerical and experimental curves. Although the valve is correctly modeled, the rest of the system presents some unmodeled behaviors. In fact, the experimental and the numerical stroke exhibit a different rising and falling slope that is more evident at higher frequencies. Moreover, for lower frequencies a saturation effect is present in the experimental

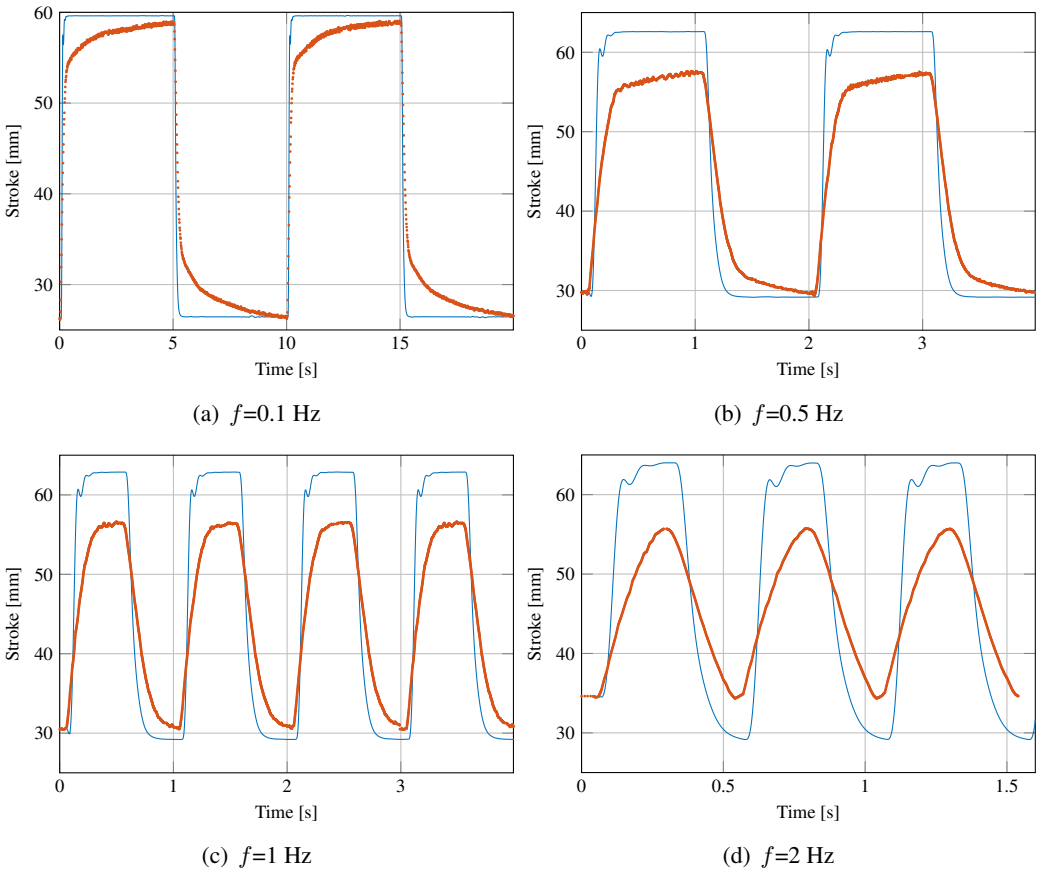

(a) f=0.1 Hz (b) f=0.5 Hz

(c) f=1 Hz (d) f=2 Hz

Figure 11: Comparison between experimental and numerical strokes for square wave command signals at different frequencies. Numerical (——) and Experimental (·····).

curve. It is probably due to resistive and capacitive phenomena that are not included in this preliminary model. For this reason the numerical model overestimates the amplitude of the stroke.

Finally, by using a square wave input with stepped variable frequency, the cylinder stroke is not able to follow the input as shown in Figure 12. A reduction of the stroke of the cylinder as the frequency increases is clearly observed: starting from 10 Hz, experimental tests revealed negligible oscillations of the cylinder rod. This is certainly due to the dynamic behavior of the proportional pressure control valve that acts as a low-pass filter.

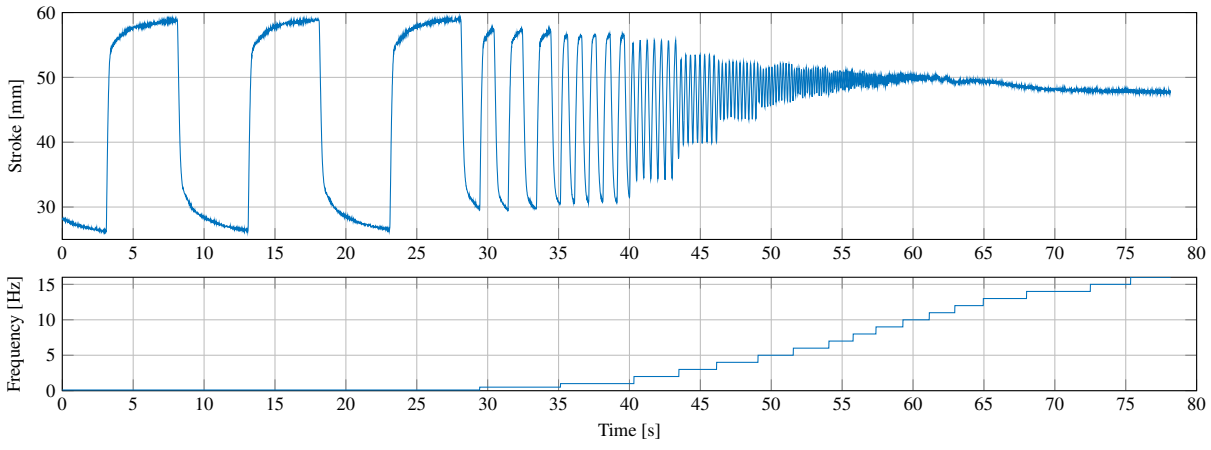

Figure 12: Cylinder stroke for square wave input with stepped variable frequency.

5 Concluding remarks

In this paper, a multi-physic modeling of a hydraulic and pneumatic active suspension systems of the operator seat of an agricultural tractor is performed. The modeling aims at providing a reliable simulator for the development and the optimization of the control system. Experimental tests are performed on a full scale testbed for the hydraulic configuration and on a reduced scale testbed for the pneumatic one. In both the hydraulic and pneumatic cases, the experimental data are compared to the results obtained from the numerical model. The hydraulic model provides a qualitatively good estimation of the vertical motion of the suspended mass, despite of slightly different amplitude. In particular, the observed experimental data suggest that some physical behavior is not fully captured by the numerical model. For the pneumatic model, an experimental identification of the electrovalve model is performed providing a reliable estimation of its dynamic behavior up to 10 Hz. The results of the simplified numerical model of the whole pneumatic system shows some discrepancies with respect to the experimental data. In this case, it seems that some physical phenomena still need to be accounted for: they will be introduced in order to try to significantly improve the model.

Acknowledgements

This research was developed in the frame of the Project No. BRiC-2019-ID14 funded by INAIL (Italian National Institute for Insurance against Accidents at Work and Occupational Diseases).

References

[1] X. Zeng, A. M. Kociolek, M. I. Khan, S. Milosavljevic, B. Bath, and C. Trask, "Whole body vibration exposure patterns in canadian prairie farmers," *Ergonomics*, vol. 60, no. 8, pp. 1064–1073, 2017.

[2] R. Stayner, *Whole-body Vibration and Shock: A Literature Review: Extension of a Study of Overtravel and Seat Suspensions*. University of Southampton, Institute of Sound and Vibration Research, 2001.

[3] J. Kim, J. Dennerlein, and P. Johnson, "The effect of a multi-axis suspension on whole body vibration exposures and physical stress in the neck and low back in agricultural tractor applications," *Applied Ergonomics*, vol. 68, pp. 80–89, 2018.

[4] H. C. Boshuizen, P. M. Bongers, and C. T. Hulshof, "Self-reported back pain in tractor drivers exposed to whole-body vibration," *International archives of occupational and environmental health*, vol. 62, no. 2, pp. 109–115, 1990.

[5] M. Bovenzi and A. Betta, "Low-back disorders in agricultural tractor drivers exposed to whole-body vibration and postural stress," *Applied ergonomics*, vol. 25, no. 4, pp. 231–241, 1994.

[6] S. K. Essien, C. Trask, M. Khan, C. Boden, and B. Bath, "Association between whole-body vibration and low-back disorders in farmers: A scoping review," *Journal of Agromedicine*, vol. 23, no. 1, pp. 105–120, 2018.

[7] M. Zehsaz, M. H. Sadeghi, M. M. Ettefagh, and F. Shams, "Tractor cabin's passive suspension parameters optimization via experimental and numerical methods," *Journal of Terramechanics*, vol. 48, no. 6, pp. 439–450, 2011.

[8] I. Hostens, K. Deprez, and H. Ramon, "An improved design of air suspension for seats of mobile agricultural machines," *Journal of Sound and Vibration*, vol. 276, no. 1, pp. 141–156, 2004.

[9] A. Soliman and M. Kaldas, "Semi-active suspension systems from research to mass-market – a review," *Journal of Low Frequency Noise, Vibration and Active Control*, vol. 40, no. 2, pp. 1005–1023, 2021.

[10] A. Nieto, A. Morales, J. Trapero, J. Chicharro, and P. Pintado, "An adaptive pneumatic suspension based on the estimation of the excitation frequency," *Journal of Sound and Vibration*, vol. 330, no. 9, pp. 1891–1903, 2011.

[11] W. East, J. Turcotte, J.-S. Plante, and G. Julio, "Experimental assessment of a linear actuator driven by magnetorheological clutches for automotive active suspensions," *Journal of Intelligent Material Systems and Structures*, vol. 32, no. 9, pp. 955–970, 2021.

[12] D. Quaini, K. Sazgetdinov, V. Ivanov, and A. Ferrara, "Optimization based sliding mode control in active suspensions: Design and hardware-in-the-loop assessment," in *2020 European Control Conference (ECC)*, 2020, pp. 1607–1612.

[13] M. H. Ab. Talib and I. Z. Mat Darns, "Self-tuning PID controller for active suspension system with hydraulic actuator," in *2013 IEEE Symposium on Computers & Informatics (ISCI)*, 2013, pp. 86–91.

[14] M. G. Antonelli, P. Beomonte Zobel, F. Durante, and F. Gaj, "Development and testing of a grasper for notes powered by variable stiffness pneumatic actuation," *International Journal of Medical Robotics and Computer Assisted Surgery*, vol. 13, no. 3, 2017.

[15] K.-H. Nam, B.-S. Kim, and J.-B. Song, "Compliant actuation of parallel-type variable stiffness actuator based on antagonistic actuation," *Journal of Mechanical Science and Technology*, vol. 24, no. 11, p. 2315 – 2321, 2010.

[16] C. Ferraresi and M. Sorli, "Modeling and analysis of pressure control systems," *Fluid*, vol. 357, pp. 58–65, 1994.